Performance Analysis of Friction Stir Welded Lightweight Aluminum Alloy Sheet

Wang Hongfeng[1,2*], Zuo Dunwen[2], Liu Shengrong[1], Pu Jiafei[1] & Song Weiwei[1,2]

[1]College of Mechanical and Electrical Engineering, Huangshan University, Huangshan, Anhui 245041, P.R. China
[2]College of Mechanical and Electrical Engineering, Nanjing University of Aeronautics and Astronautics, Nanjing, Jiangsu 210016, P.R. China
[*]E-mail: wanghnfeng@163.com

Highlights:

- This work mainly studied the microstructure, tensile strength, hardness, wear resistance and corrosion resistance of the friction stir welding area on a lightweight aluminum alloy sheet.
- The tensile strength of the welded zone when the rotation speed of the tool was 15000 rpm and the advancing speed of the tool was 300 mm·min^{-1} obtained was highest, i.e. 74.8% of the base metal.
- The friction coefficient of the welded zone obtained under each parameter was smaller than that of the base metal.

Abstract. The present research envisaged the performance analysis of a 1-mm thick 6061-T6 aluminum alloy sheet welded by the friction stir welding technique, using optical microscopy, micro-hardness measurement, a tensile test, a friction and wear test, and a salt spray corrosion test. It was found that the grain in the welded zone obtained was refined under each parameter. When the rotating speed of the tool was 15,000 rpm and the traveling speed of the tool was 300 mm·min^{-1}, the tensile strength of the welded zone was highest, i.e. 74.8% of the base metal. Furthermore, the hardness distribution curve of the welded zone was of the 'W' type under each parameter, but the hardness value was lower than that of the base metal. The friction coefficient of the welded zone was lower than that of the base metal under each parameter, and the wear form was found to be mainly adhesive wear accompanied by abrasive wear. The welded zone and the base metal were subjected to salt spray corrosion after 12 hours under each parameter, which had a negative effect on the quality. However, after 12 hours of subsequent corrosion, the quality of each sample and the base material was not obvious.

Keywords: *aluminum alloy; corrosion resistance; friction stir welding; microstructure; tensile strength; wear resistance.*

Received October 28th, 2019, Revised February 21st, 2020, Accepted for publication September 17th, 2020.
 ISSN: 2337-5779,
DOI: 10.5614/j.eng.technol.sci.2020.52.6.4

1 Introduction

Aluminum alloys can be processed into various structural parts for new-energy vehicles, leading to an effective reduction in the weight of automobiles. They are widely favored in new-energy vehicle manufacturing due to their low density and high strength [1-2]. On the other hand, aluminum alloys are difficult to weld by conventional fusion welding [3-6]. The process of riveting can achieve joining but increases the weight and the riveting openings can seriously affect the service life of structural parts [7-9]. Friction stir welding (FSW) is a solid state joining technique developed for joining Al-alloys, in which a rotating tool plunges the sheets to be welded, stirs them together and travels them through a joint line [9-10]. Numerous studies have been conducted on FSW of Al-alloys in recent years and it is well documented that this joining technique can produce defect-free joints of aluminum alloys [11-20]. However, optimum weld parameters should be used for the procedure to be successful. Otherwise, some weld defects, such as tunnel-like cavity or kissing bonds, can be encountered in FSW [21-27].

Friction stir welding of aluminum alloy sheets has not been studied extensively in the literature. Simoncini, *et al.* [28] used a tool with shoulder diameters of 19 mm and 8 mm to friction stir an AA5754 aluminum alloy sheet. Leal, *et al.* [29] employed a 5-mm diameter concave tapered shoulder tool and a 7-mm diameter double spiral shoulder tool to friction stir 1-mm thick AA5182-H111 and AA6016-T4 aluminum alloys. The results showed that an 'onion ring' appeared in the welded area with the concave tapered shoulder, which did not appear in the welded area of the double spiral shoulder. He Diqi, *et al.* [30] used a tool with a shoulder diameter of 6 mm to agitate and frictionally connect a 2024-T4 aluminum alloy sheet with a thickness of 1.8 mm and control the warpage of the sheet by a water mist cooling device. The results showed that the welding area was perfectly formed, with no defects inside. Chen, *et al.* [31] used a tool with a 6-mm diameter shoulder to friction stir a 1-mm thick 2014 aluminum alloy sheet, where the defect in the welded area gradually disappeared and the mechanical properties were stabilized when the rotation speed of the tool was higher than 15,000 rpm and the traveling speed of the tool was 50-170 mm/min. Rodrigues, *et al.* [32] used a stirrer with a diameter of 10 mm and 14 mm with and without heating a 1-mm thick 6061-T4 aluminum alloy sheet.

The results showed that the heating assisted friction stir-welding zone was superior to the unheated friction stir-welding zone. Earlier studies, where the welded width of aluminum alloy sheets was greater than 4 mm, indicated that when the thickness of the sheet was about 1 mm, the friction stir welding width was 4 mm and good welding performance was difficult to realize. In this study, friction stir welding of 1-mm thick 6061-T6 aluminum alloy was performed with a 4-mm shoulder head. The influence of different process parameters on the

performance of the welded zone was studied to provide theoretical support for practical engineering applications.

2 Experimental Materials, Equipment and Methods

2.1 Experimental Materials

In this study, a 1-mm thick 6061-T6 aluminum alloy sheet was employed, which was subjected to a solution heat treatment for artificial aging. The specific chemical composition is shown in Table 1. The tensile strength, σb, of the material was 330 MPa and the elongation, δ, was 12.9%. The test plate size was 200 mm × 100 mm × 1 mm; two plates were welded together.

Table 1 Chemical composition of 6061-T6 aluminum alloy (mass fraction,%).

Mg	Si	Fe	Cu	Mn	Cr	Zn	Ti	Al
0.762	0.6	0.31	0.02	0.08	0.01	0.04	0.03	Balance

2.2 Experimental Equipment and Processes

The experiment employed FSW-LS-A02 friction stir welding equipment. The tool adopted a conical shape with a shoulder diameter of 4 mm. The end face was designed with a concave ring-shaped groove and the probe was 0.8 mm, the root diameter was 1.5 mm, the top diameter was 1.2 mm, and the stirring head material was H13 die steel, as shown in Figure 1. A metallographic sample measuring 15 × 6 × 1 mm was cut along the specimen perpendicular to the welded direction, inlaid and polished. Subsequently, it was etched using Keller reagent for 2 min, washed and dried to observe the microstructure under a metallographic microscope. The tensile specimen size was carried out in accordance with the national standard GB/T228-2002 and the experiment was carried out in a WDW-50E miniature control electronic universal testing machine with tensile rate at 1 mm/min. The tensile fracture morphology was observed by a Hitachi S-4800 scanning electron microscope. A hardness test was performed on a vertical welding area and the five-point measurement method was used with the welding center as the axis of symmetry. The distance between the hardness test points was 1 mm.

The hardness was measured using an HV-1000 Vickers hardness tester. The experimental loading force was 300 gf, the loading time was 10 s, and each point was measured 5 times. The average value was calculated as the final hardness value. A friction and wear sample with a size of 10 × 6 × 1 mm was cut out of the welded sample, as shown in Figure 2. A friction and wear test was performed using a CFW-1M microcomputer controlled coating friction and wear testing

machine. The samples on the friction pair were the 6061-T6 aluminum alloy friction stir welding zone and the base metal, and the lower sample was 45 steel. The friction and wear test was carried out in a wet state. The wet medium was lubricated at a rate of 1 mL/min into the friction surface. The sample was circumferentially slid relative to the disk and a vertical load of 368 g was applied to the sample. The rotation rate was 100 rpm and the rotation time was 6 min. During the experiment, an AR124CN electronic balance was used to record the mass before and after the friction and wear samples. According to the friction data and the friction curve, the average friction coefficient was determined.

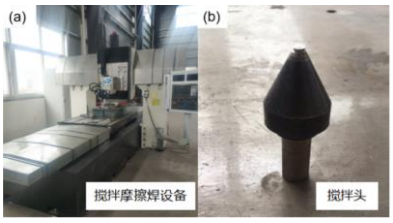

Figure 1 Friction stir welding device and stirring tool.

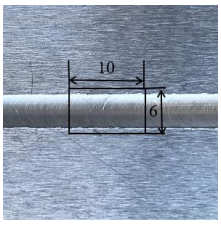

Figure 2 Friction and wear sample interception position.

The salt spray corrosion sample was the same as the wear sample, which was placed in a JY-60-SS salt spray corrosion chamber. The experiment was carried out by continuous spraying on the hanging piece. The etching solution used was 5% ± 0.5% NaCl solution, the pH range was 6.5~7.2, and the temperature of the box was controlled at (35 ± 1°C). The sample was removed every 12 h during the corrosion process. The corrosion degree was analyzed based on weight loss before and after corrosion. During the experiment, the angle of the tool was 2° and the amount of pressure under the shoulder was 0.1 mm. The specific test parameters and numbers are shown in Table 2.

Table 2 FSW test process parameters.

Sample number	Rotating speed of the tool (ω/rpm)	Advancing speed of the tool (v/mm·min^{-1})
1	8,000	100
2	8,000	200
3	8,000	300
4	10,000	100
5	10,000	200
6	10,000	300
7	15,000	100
8	15,000	200
9	15,000	300

Before the experiment, the aluminum alloy sheet was polished with sandpaper to remove the surface oxide layer. Subsequently, the surface was cleaned with absolute ethanol and the oil was removed and blow-dried. Finally, the surface was mounted on a fixture, the welding area was aligned and the friction stir welding experiment was performed. The tool was rotated counter-clockwise.

3 Analysis of Experimental Results

3.1 Metallographic Analysis

Figure 3 shows the metallographic structure of the welded area of each sample. It can be seen from the figure that no matter what joining process parameters were selected, the grains of the welded zone were recrystallized and refined, and were equiaxed.

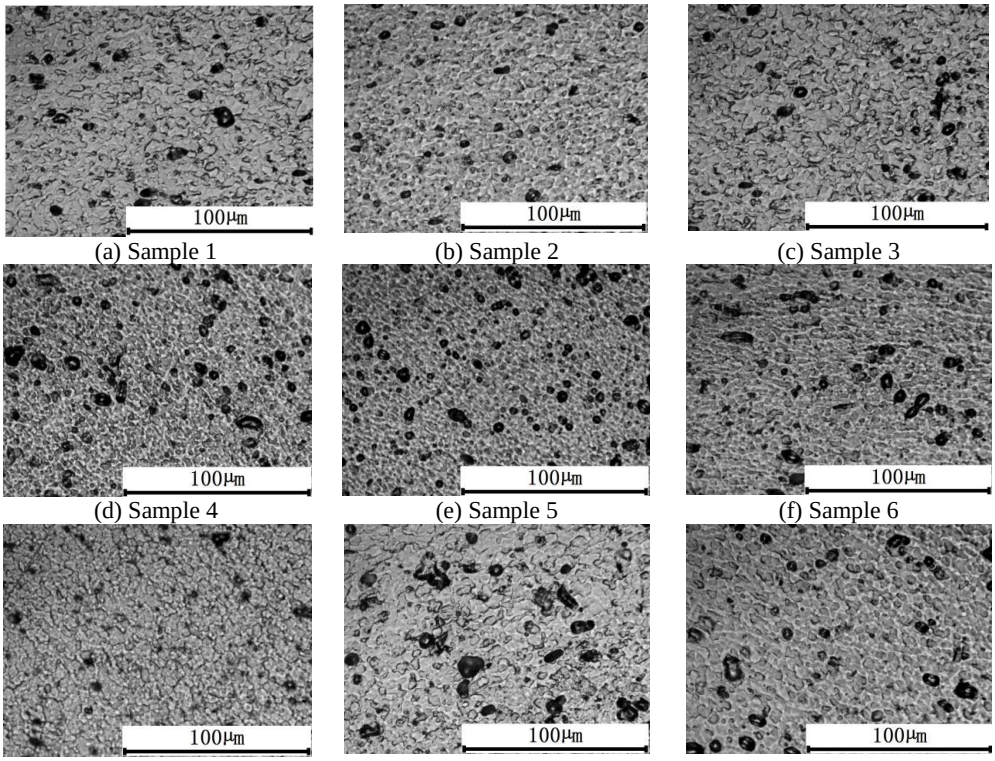

(a) Sample 1 (b) Sample 2 (c) Sample 3

(d) Sample 4 (e) Sample 5 (f) Sample 6

(g) Sample 7 (h) Sample 8 (i) Sample 9

Figure 3 Metallographic structures of the welding area.

At a constant traveling speed of the tool, when the rotational speed of the tool was increased, the degree of refinement of the grain in the welded zone initially

increased and later decreased. When the rotational speed of the tool was constant, with an increase in the traveling speed of the tool, the grain of the joining zone was first refined and then increased. All samples exhibited a smaller grain size than the base metal, as shown in Figure 4.

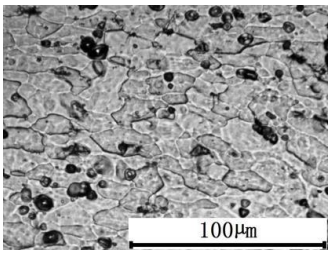

Figure 4 Metallographic structure of base metal.

Figure 5 shows the metallographic structure of each position of the welded zone of Sample 9. It can be clearly seen from Figures 5 (a) and (c) that stirred zones, including equiaxed crystals and plate crystals, appeared in the affected area of the heat engine, while heat-affected zones were absent in Figures 5(b) and (d). This is because the material in the heat-affected zone is strongly squeezed by the agitator head shoulder, the table and the material surrounding the plate.

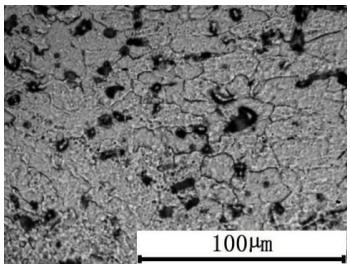

(a) Advancing side heat engine affected zone

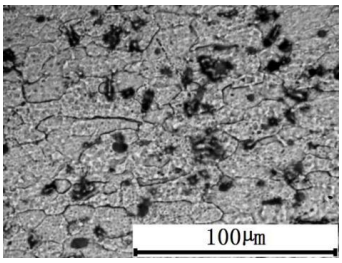

(b) Forward side heat affected zone

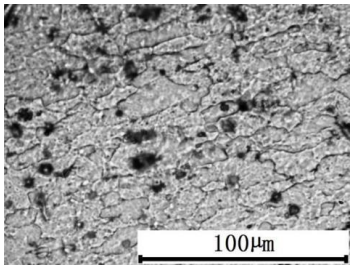

(c) Retreating side heat engine affected zone

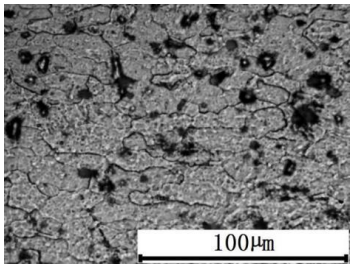

(d) Retreating side heat affected zone

Figure 5 Metallographic structure of Sample 9.

In Figure 5, the grain size of the heat-affected zone of the advancing side and the retreating side were basically the same, indicating that the temperature on the advancing side and the retreating side of the thin-plate 6061 aluminum alloy FSW was almost the same. Furthermore, the grains in the heat-affected zone were substantially identical to those in the parent metal. The metallographic structure of the welded zone of the other samples was basically the same as that in Figure 5, except that there was a slight change in grain size.

3.2 Tensile Properties of the Joining Area

Table 3 shows the results of the tensile test of the samples. It can be seen from the table that the tensile strength of the welded samples obtained under each parameter was lower than that of the base metal. When the rotating speed of the tool was 15,000 rpm and the advancing speed of the tool was 300 mm·min^{-1}, the tensile strength of the welded zone was highest (247 MPa), i.e. 74.8% of the base metal. When the rotating speed of the tool was 8,000 rpm and the advancing speed of the tool was 200 mm·min^{-1}, the elongation was highest, i.e. 8.4% (reaching 65.1% of that of the base metal). When the rotation speed of the tool was 10,000 rpm and the advancing speed of the tool was 100 mm·min^{-1}, the tensile strength of the welded area and the lowest elongation were 190 MPa and 4.9%, respectively, i.e. only 57.6% and 38%, respectively of that of the base metal. The tensile fracture position of the connected specimen obtained by each parameter was mostly concentrated in the center of the welded region, which may be related to the reduction of the thickness of the metal material caused by shoulder extrusion during the stirring process [33], thereby making the region a weak mechanical region. Hence, several fractures occurred in this area. A small fault occurred in the welding area of the retreating side of the heat engine affected zone and in the heat-affected zone, which was due to the uneven grain variations in this area.

Table 3 Tensile strength and elongation of the welded area.

Sample number	Tensile strength (Mpa)	Elongation (%)	Break position
1	202	7.9	Welding area center
2	213	8.4	Retreating side
3	205	6.5	Retreating side
4	190	4.9	Welding area center
5	215	5.5	Welding area center
6	203	5.4	Welding area center
7	202	5.6	Welding area center
8	232	5.2	Welding area center
9	247	5.3	Welding area center

The two sets of welded specimens with the highest elongation and the lowest elongation in the tensile test were selected, and the fractures of the tensile specimens were observed separately to obtain the tensile fracture profile, as shown in Figure 6. It can be seen from Figure 6(a) that there was a large number of dimples in the fracture of the tensile specimen and there were obvious tearing ribs near the dimples.

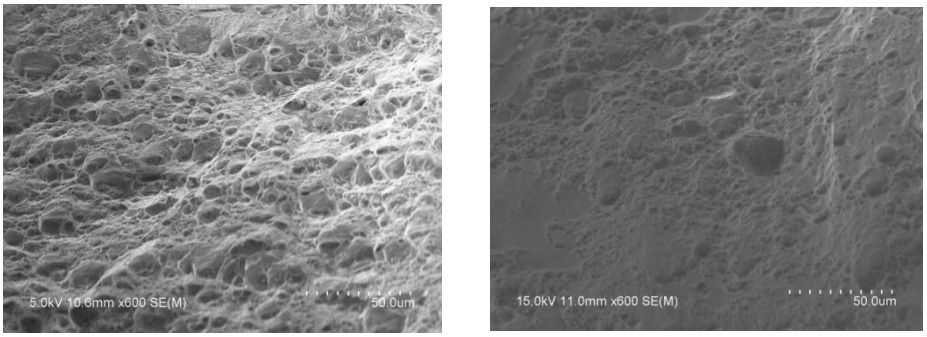

(a) At a rotation speed of 8,000 rpm and an advancing speed of 200 mm·min^{-1}

(b) At a rotation speed of 10,000 rpm and an advancing speed of 100 mm·min^{-1}

Figure 6 Fracture morphology of the fracture surface of the welded specimen.

The number of dimples was large and the distribution was dense, indicating that the welded region exhibited good plasticity and the fracture was a typical plastic fracture. Figure 6(b) shows that the fracture was smooth and flat, the dimples were small and the depth was shallow. The fracture form was mainly a brittle fracture and a small amount of plastic fracture was stirred.

3.3 Microhardness of the Joining Area

Figure 7 contains a graph showing the surface hardness test of the welded area obtained by different joining parameters. It can be seen from the figure that the surface hardness test curve of the welded area obtained under each parameter was basically symmetrical and the curve shape was like a 'W'. After the stirring of the pin, the hardness of the stirring zone was a little low and the hardness of the stirring section of the tool was improved, but the hardness was lower than that of the base material (the base material's hardness was 115 HV). Since equiaxed crystals appeared in the welded region, the hardness should have theoretically improved, but the base metal was extruded and the formed elongated long crystal grains exhibited a higher hardness than the simple equiaxed crystal surface.

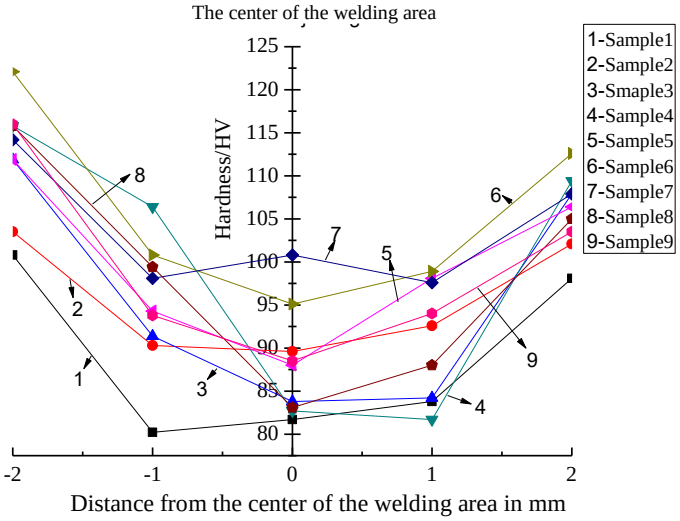

Figure 7 Hardness curves of each sample.

3.4 Analysis of Wear Resistance

Figure 8 shows a graphical representation of the friction coefficient for different samples and base materials. It can be seen from Figure 8 that the average friction coefficients of Sample 1 to Sample 9 and the base material were 0.1368, 0.3071, 0.1398, 0.5620, 0.2116, 0.4172, 0.3530, 0.1946, 0.2881 and 0.6141, respectively. The average friction coefficient of each sample was lower than that of the base material due to the grain refinement of the friction stir welding regions of the respective samples. However, there was still a difference between the friction coefficient in Figure 8 and the hardness value in Figure 7, which indicates that the hardness value was not the only criterion for measuring the friction coefficient.

Figures 9 and 10 present SEM photographs of the wear scars for each sample and the base material, respectively. It can be seen from Figure 9 that the friction and wear form of each sample were mainly adhesive wear and the auxiliary belt exhibited a certain amount of abrasive wear. The wear photos in Figure 9 are basically the same as the friction coefficient curve in Figure 8.

It can be seen from Figure 10 that the wear of the base metal was serious and the base material had a large amount of furrow wear accompanied by abrasive wear.

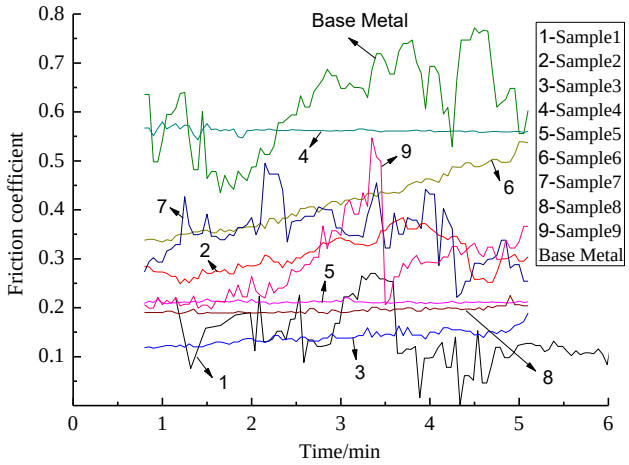

Figure 8 Friction coefficients of each sample and base metal.

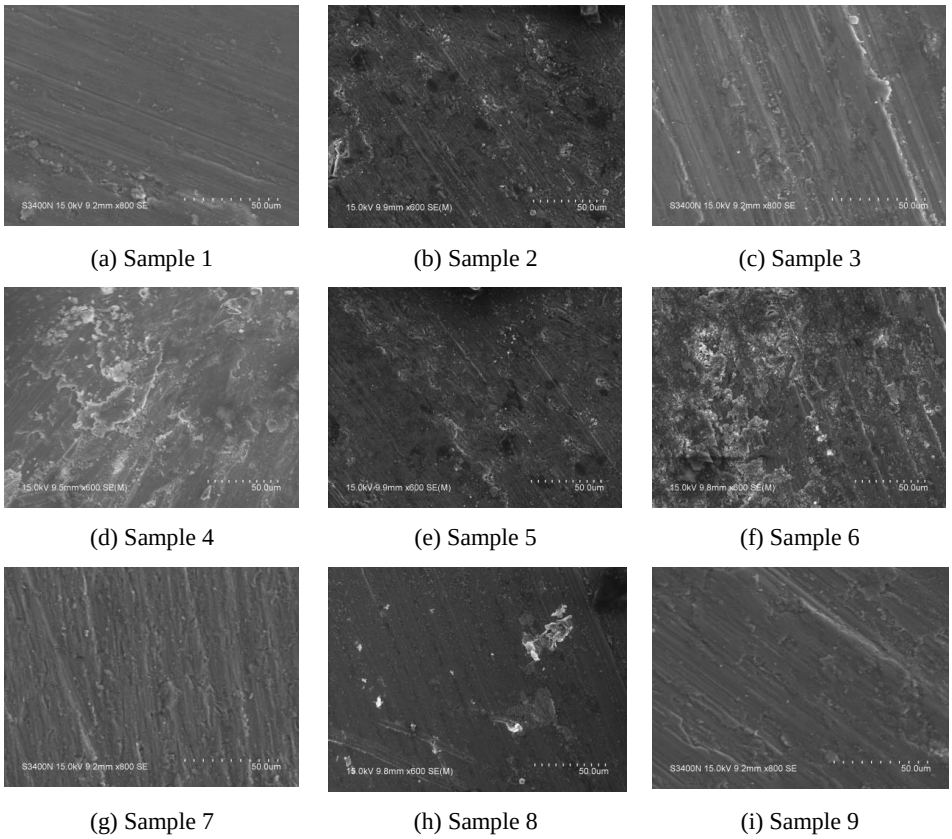

(a) Sample 1 (b) Sample 2 (c) Sample 3

(d) Sample 4 (e) Sample 5 (f) Sample 6

(g) Sample 7 (h) Sample 8 (i) Sample 9

Figure 9 SEM morphology of each sample.

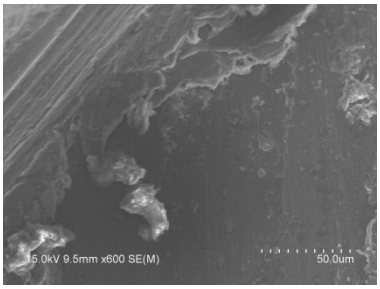

Figure 10 SEM morphology of the base metal.

3.5 Analysis of Salt Spray Corrosion

Table 4 shows the quality of the different samples after the salt spray corrosion test at different time periods. It can be seen from Table 4 that for every 12 hours of salt spray corrosion of each sample and the base material, the quality of the corresponding sample decreased, with a minor increase at 48 h, which may be due to corrosion product adhering the corrosion surface. However, all samples showed a decrease in mass after 48 hours of salt spray corrosion, indicating that the corrosion occurred due to the salt spray in each sample. However, the corrosion degree of the samples obtained by different parameters was different.

Table 4 Corrosion quality of each sample and parent metal at different time periods.

Sample number	Pre-corrosion quality (g)	Quality after 12 h corrosion (g)	Quality after 24 h corrosion (g)	Quality after corrosion for 36 h (g)	Quality after corrosion for 48 h (g)
1	0.094	0.091	0.092	0.090	0.091
2	0.121	0.107	0.105	0.104	0.105
3	0.102	0.099	0.097	0.097	0.099
4	0.106	0.108	0.107	0.105	0.103
5	0.108	0.103	0.106	0.105	0.105
6	0.103	0.098	0.101	0.099	0.098
7	0.104	0.1	0.1	0.101	0.101
8	0.11	0.106	0.105	0.107	0.108
9	0.118	0.116	0.115	0.115	0.116
Base metal	0.136	0.134	0.133	0.132	0.132

Furthermore, in the case of Sample 2, when the rotating speed of the tool was 8,000 rpm and the advancing speed of the tool was 200 mm·min^{-1}, the salt fog corrosion weight loss was most obvious.

After 48 hours of salt spray corrosion, except for Samples 2 and 6, the corrosion quality of each sample was lower than that of the base material, indicating that the welded samples obtained under these parameters were more resistant to corrosion than the base metal. After the end of the salt spray corrosion, the corrosion rate during the entire corrosion of the sample was studied with reference to the static weight loss method [34]. The salt spray corrosion test data are shown in Table 5. The corrosion rate, V, can be calculated by Eq. (1):

$$V = (m_0\text{-}m_1)/(s\times t) \tag{1}$$

where m_0 represents the mass of the sample before the corrosion test; m_1 represents the mass of the sample after the corrosion test; s represents the total area of the sample exposed to the corrosive medium; and t is the time of the corrosion test. The results in Table 5 were consistent the results in Table 4.

Table 5 Results of salt spray corrosion test for parent metal and welding area.

Sample number	$s\times10^{-6}$m^2	m_0(g)	m_1(g)	t/h	V(g/(m^{2}h))
1	49.5	0.094	0.091	48	1.263
2	57	0.121	0.105	48	5.848
3	52.25	0.102	0.099	48	1.196
4	52.25	0.106	0.103	48	1.196
5	50	0.108	0.105	48	1.250
6	52.25	0.103	0.098	48	1.994
7	49.5	0.104	0.101	48	1.263
8	57	0.110	0.108	48	0.731
9	60	0.118	0.116	48	0.694
Base metal	55	0.136	0.132	48	1.515

4 Conclusion

In the present study, a 1-mm thick 6061-T6 aluminum alloy sheet welded by the friction stir welding technique was analyzed for its performance using optical microscopy, micro-hardness measurement, a tensile test, a friction and wear test, and a salt spray corrosion test. Our study offers the following major conclusions:

1. The grain of the welded zone obtained under each parameter was refined and at a constant advancement speed, with an increase in the rotation speed of the tool, the degree of refinement of the grain in the welded zone initially increased and later decreased. When the rotation speed of the tool was constant, as the advancement speed of the tool increased, the grain of the welded zone was first refined and then increased.
2. The tensile strength of the welded specimen obtained under each parameter was lower than that of the base metal. When the rotation speed of the tool was 15,000 rpm and the advancing speed of the tool was 300 mm·min^{-1}, the tensile strength of the welded zone obtained was highest, i.e. 74.8% of the

base metal. When the rotating speed of the tool was 10,000 rpm and the advancing speed of the tool was 100 mm·min^{-1}, the tensile strength of the welded zone obtained was lowest, i.e. 57.6% of the base metal. The hardness of the welded zone obtained under each parameter was smaller than that of the base metal and both curves had a 'W' shape.

3. The friction coefficient of the welded zone obtained under each parameter was smaller than that of the base metal and the wear caused was mainly adhesive wear accompanied by abrasive wear.
4. The welded zone and the base metal obtained by each sample passed the salt spray corrosion test. The quality of the welded sample and the base metal decreased after 12 hours of corrosion and the loss in mass at the subsequent corrosion sample was not significant.

Acknowledgements

This study was supported by the Key Research and Development Project from Anhui Province of China (Grant No. 1704a0902053); the Key Natural Science Foundation of Anhui Higher Education Institutions of China (Grant No. KJ2016A681); the Major Natural Science Foundation of Anhui Higher Education Institutions of China (Grant No. KJ2016SD55); and the Open Research Project of Anhui Simulation Design and Modern Manufacture Engineering Technology Research Center (Huangshan University) (NO. SGCZXZD1801).

References

[1] Xiang, J.F. & Wei, J.H., *Analysis of the Status Quo and Development of New Energy Vehicles*, The Journal of Hubei Agricultural Mechanization, (04), pp. 21, 2019. (Text in Chinese and Abstract in English)

[2] Wang, H.B. & He, C.X., *Application of Aluminum Body Plate in Automobile Lightweight*, World Nonferrous Metals, (07), pp. 186-187, 2018. (Text in Chinese and Abstract in English)

[3] Çam, G., Ventzke, V., Dos Santos, J.F., Koçak, M., Jennequin, G., Gonthier-Maurin, P., Penasa, M. & Rivezla, C., *Characterization of Laser and Electron Beam Welded Al-Alloys*, Praktische Metallographie, **36**(2), pp. 59-89, 1999.

[4] Çam, G., Ventzke, V., Dos Santos, J.F., Koçak, M., Jennequin, G. & Gonthier-Maurin, P., *Characterisation of Electron Beam Welded Aluminium Alloys*, Science and Technology of Welding and Joining, **4**(5), pp. 317-323, 1999.

[5] Çam, G. & Koçak, M., *Microstructural and Mechanical Characterization of Electron Beam Welded Al-Alloy 7020*, Journal of Materials Science, **42**(17), pp. 7154-7161, 2007.

[6] Pakdil, M., Çam, G., Koçak, M. & Erim, S., *Microstructural and Mechanical Characterization of Laser Beam Welded AA6056 Al-Alloy*, Materials Science and Engineering: A, **528**(24), pp. 7350-7356, 2011.
[7] Guo, J.F., Chen, H.C., Sun, C.N., Bi, G., Sun, Z. & Wei, J., *Friction Stir Welding of Dissimilar Materials Between AA6061 and AA7075 Al Alloys Effects of Process Parameters*, Materials and Design, **56**, pp. 185-192, 2013.
[8] Peng, Z.J., *Study on Needle-free Friction Stir Welding Process and Microstructure Analysis of 6061 Aluminum Alloy Sheet*, Master dissertation, Chongqing Jiaotong University, Chongqing, 2017. (Text in Chinese and Abstract in English)
[9] Yang, X.W., Fu, T. & Li, W.Y., *Friction Stir Spot Welding: A Review on Joint Macro-and Microstructure, Property, and Process Modelling*, Advances in Materials Science and Engineering, (1), pp. 1-11, 2014.
[10] Li, D.X., Yang, X.Q., Cui, L., He, F.Z. & Shen, H., *Effect of Welding Parameters on Microstructure and Mechanical Properties of AA6061-T6 Butt Welded Joints by Stationary Shoulder Friction Stir Welding*, Materials & Design, **64**, pp. 251-260, 2014.
[11] Kashaev, N., Ventzke, V. & Çam, G., *Prospects of Laser Beam Welding and Friction Stir Welding Processes for Aluminum Airframe Structural Applications*, Journal of Manufacturing Processes, **36**, pp. 571-600, 2018.
[12] Çam, G. & İpekoğlu, G., *Recent Developments in Joining of Aluminium Alloys*, International Journal of Advanced Manufacturing Technology, **91**(5-8), pp. 1851-1866, 2017.
[13] Çam, G., *Friction Stir Welded Structural Materials: Beyond Al-Alloys*, International Materials Reviews, **56**(1), pp. 1-48, 2011.
[14] Çam, G., İpekoğlu, G., Küçükömeroğlu, T. & Aktarer, S.M., *Applicability of Friction Stir Welding to Steels*, Journal of Achievements in Materials and Manufacturing Engineering, **80**(2), pp. 65-85, 2017.
[15] Çam, G. & Mıstıkoğlu, S., *Recent Developments in Friction Stir Welding of Al-Alloys*, Journal of Materials Engineering and Performance, **23**(6), pp. 1936-1953, 2014.
[16] Çam, G., İpekoğlu, G. & Serindağ, H.T., *Effects of Use of Higher Strength Interlayer and External Cooling on Properties of Friction Stir Welded AA6061-T6 Joints*, Science and Technology of Welding & Joining, **19**(8), pp. 715-720, 2014.
[17] İpekoğlu, G. & Çam, G., *Effects of Initial Temper Condition and Postweld Heat Treatment on the Properties of Dissimilar Friction-Stir-Welded Joints between AA7075 and AA6061 Aluminum Alloys*, Metallurgical & Materials Transactions A, **45**(7), pp. 3074-3087, 2014.
[18] İpekoğlu, G., Erim, S. & Çam, G., *Investigation into the Influence of Post-Weld Heat Treatment on the Friction Stir Welded AA6061 Al-Alloy Plates*

with Different Temper Conditions, Metallurgical & Materials Transactions A, **45**(2), pp. 864-877, 2014.

[19] İpekoğlu, G., Erim S. & Çam, G., *Effects of Temper Condition and Post Weld Heat Treatment on the Microstructure and Mechanical Properties of Friction Stir Butt Welded AA7075 Al-Alloy Plates*, International Journal of Advanced Manufacturing Technology, **70**(1), pp. 201-213, 2014.

[20] Bozkurt, Y., Salman, S. & Çam, G., *The Effect of Welding Parameters on Lap-Shear Tensile Properties of Dissimilar Friction Stir Spot Welded AA5754-H22/2024-T3 Joints*, Science and Technology of Welding and Joining, **18**(4), pp. 337-345, 2013.

[21] Çam, G., Güçlüer, S., Çakan, A. & Serindağ, H.T., *Mechanical Properties of Friction Stir Butt-Welded Al-5086 H32 Plate*, Materialwissenschaft Und Werkstofftechnik, **40**(8), pp. 638-642, 2009.

[22] İpekoğlu, G., Erim, S., GörenKıral, B. & Çam, G., *Investigation into the Effect of Temper Condition on Friction Stir Weldability of AA6061 Al-Alloy Plates*, Kovove Materialy, **51**(3), pp. 155-163, 2013.

[23] İpekoğlu, G., GörenKıral, B., Erim, S. & Çam, G., *Investigation of the Effect of Temper Condition on Friction Stir Weldability of AA7075 Al-Alloy Plates*, Materiali in Tehnologije, **46**(6), pp. 627-632, 2012.

[24] Çam, G., Serindag H.T., Çakan, A., Mistikoglu S. & Yavuz H., *The Effect of Weld Parameters on Friction Stir Welding of Brass Plates*, Materialwissenschaft Und Werkstofftechnik, **39**(6), pp. 394-399, 2008.

[25] Çam, G., Mistikoglu, S. & Pakdil, M., *Microstructural and Mechanical Characterization of Friction Stir Butt Joint Welded 63%Cu-37%Zn Brass Plate*, Welding Journal, **88**(11), pp. 225-232, 2009.

[26] Günen, A., Kanca, E., Demir, M., Çavdar, F., Mistikoğlu, S. & Çam, G., *Microstructural and Mechanical Properties of Friction Stir Welded Pure Lead*, Indian Journal of Engineering & Materials Sciences, **25**(1), pp. 26-32, 2018.

[27] Küçükömeroğlu, T., Şentürk, E., Kara, L., İpekoğlu, G. & Çam, G., *Microstructural and Mechanical Properties of Friction Stir Welded Nickel-Aluminum Bronze (NAB) Alloy*, Journal of Materials Engineering and Performance, **25**(1), pp. 320-326, 2016.

[28] Simoncini, M., Ciccarelli, D., Forcellese, A. & Pieralisi, M., *Micro- and Macro- Mechanical Properties of Pinless Friction Stir Welded Joints in AA5754 Aluminium Thin Sheets*, Procedia Cirp, **18**, pp. 9-14, 2014.

[29] Leal, R.M., Leitão, C., Loureiro, A., Rodrigues, D.M. & Vicaça, P., *Material Flow in Heterogeneous Friction Stir Welding of Thin Aluminium Sheets: Effect of Shoulder Geometry*, Materials Science and Engineering: A, **498**(1), pp. 384-391, 2008.

[30] He, D.Q., Li, S.P., Li, J. & He, X.J., *Friction Stir Welding of 1.8mm 2024-t4 Aluminum Alloy Plate. Hot Working Process*, **40**(7), pp. 112-114, 2011. (Text in Chinese and Abstract in English)

[31] Chen, S., Zhou, Y., Xue, J.R., Ni, R.Y., Guo, Y. & Dong, J.H., *High Rotation Speed Friction Stir Welding for 2014 Aluminum Alloy Thin Sheets*, Journal of Materials Engineering and Performance, **26**(3), pp.1337-1345, 2017.

[32] Rodrigues, D.M., Loureiro, A., Leitao, C., Leal, R.M., Chaparro, B.M. & Vilaça, P., *Influence of Friction Stir Welding Parameters on the Microstructural and Mechanical Properties of AA 6016-T4 Thin Welds*, Materials and Design, **30**(6), pp. 1913-1921, 2009.

[33] Tong, J.H., Li, L., Deng, D. & Wan, F.R., *Friction Stir Welding of Aluminum Alloy Sheet 6061-T6*, Journal of University of Science and Technology Beijing, (9), pp. 1011-1017, 2008. (Text in Chinese and Abstract in English)

[34] Ye, K.M., *Introduction to Metal Corrosion and Protection*, Beijing: Higher Education Press, 1993.